Environ. Sci. Technol. **2002**, *36,* 1460−1466

Mechanisms of Selenate Adsorption on Iron Oxides and Hydroxides

D. PEAK* AND D. L. SPARKS

Department of Plant and Soil Sciences, University of Delaware, 149 Townsend Hall, Newark, Delaware 19717-1303

Selenate (SeO_4^{2-}) is an oxyanion of environmental importance because of its toxicity to animals and its mobility in the soil environment. It is known that iron(III) oxides and hydroxides are important sorbents for SeO_4^{2-} in soils and sediments, but the mechanism of selenate adsorption on iron oxides has been the subject of intense debate. Our research employed Extended X-ray absorption fine structure and attenuated total reflectance−Fourier transform infrared spectroscopies to determine SeO_4^{2-} bonding mechanisms on hematite, goethite, and hydrous ferric oxide (HFO). It was learned that selenate forms only inner-sphere surface complexes on hematite but forms a mixture of outer- and inner-sphere surface complexes on goethite and HFO. This continuum of adsorption mechanisms is strongly affected by both pH and ionic strength. These results suggest that adsorption experiments should be conducted on several different iron oxides and over a wide range of reaction conditions to accurately assess the reactivity of oxyanions on iron oxides.

Introduction

Selenate (SeO_4^{2-}(aq)) is the fully oxidized form of selenium and is often seen in aerated soils. Selenium is an essential micronutrient for animals, but when soil selenate levels are high, it often accumulates in plants and can prove toxic to animals that ingest the vegetation. Alternatively, deficiency symptoms are commonly seen when selenium levels in plants are low (*1*). Therefore, understanding the chemistry of selenate in soils is important for minimizing potentially hazardous environmental effects. Selenate is a weakly basic group VI oxyanion and typically exists in natural aqueous systems as either the fully deprotonated form or the singly protonated biselenate ($HSeO_4^-$(aq)) (*2*). Both of these ions have a hydrated radius of ∼4 Å (*3*). The pK_a for the protonation reaction is ∼1.9, making the fully deprotonated form the dominant ion under normal soil conditions.

Column studies that monitored selenate leaching through soils (*4*) reported that selenate was very weakly bound and could be completely leached from soils in a short period of time. The soils studied were sandy loam soils low in iron oxides with smectites being the predominant clay minerals. Other researchers (*5*) reported only slight sorption of selenate to kaolinite and montmorillonite as a function of pH. Furthermore, selenate adsorption was found to be negligible on alluvial soils by Neal and Sposito (*6*). None of the above studies utilized soils with a significant iron oxide component however. Adsorption reactions of selenate with naturally occurring iron oxide minerals and amorphous iron hydroxide coatings may be substantial in soils that are slightly acidic due to their positive charge (PZC of 6−7 in the presence of carbonate) and high surface area.

Unfortunately, little macroscopic and modeling data are available in the literature for selenate adsorption on iron oxides. Davis and Leckie (*7*) showed that pH envelopes for sulfate and selenate adsorption on ferrihydrite are identical. This suggests that both sorbates have the same affinity for the surface and implies that the same mechanisms are present in both systems. Zhang and Sparks (*1*) analyzed selenate adsorption on goethite using a triple-layer model and pressure jump relaxation and found results consistent with outer-sphere complexation of selenate. Yamaguchi and colleagues (*8*) compared volume changes due to sulfate and selenate adsorption on an amorphous iron oxide using dilatometry. The volume changes for sulfate and selenate were identical, again suggesting that similar reaction mechanisms were occurring with these ions. A large loss of waters of hydration was observed in both ions, which suggests that a ligand-exchange reaction occurred at the iron oxide's surface. Su and Suarez (*9*) found that selenate adsorption on both goethite and amorphous iron hydroxide shifted PZC to lower values using electrophoretic mobility. This would also suggest an inner-sphere adsorption mechanism. They also found a large ionic strength dependence on pH envelopes with adsorption suppressed as ionic strength increased. This seemingly contradictory observation suggests an outer-sphere adsorption mechanism, but it was also noted that as selenate concentration in solution was increased that this ionic strength dependence became much smaller.

Early studies utilizing ex situ FTIR techniques observed inner-sphere bidentate binuclear complexes of selenate on iron oxides (*10*). However, these studies involved extensive sample modification such as drying and subjection to vacuum. Such preparation may force inner-sphere surface complexes by removing waters of hydration from the mineral surface (*11*) and has been shown to cause a conversion from monodentate to bidentate surface complexes (*12*). Hayes and colleagues (*13*) used EXAFS to study the adsorption mechanisms of selenate and selenite on goethite in situ and concluded that selenate adsorbs to goethite via an outer-sphere mechanism. In stark contrast, Manceau and Charlet (*14*) conducted EXAFS experiments at the same pH and surface coverage as Hayes et al. (*13*) and concluded that selenate forms inner-sphere complexes (bidentate binuclear and bidentate mononuclear) on both goethite and hydrous ferric oxide. Su and Suarez (*9*) used both attenuated total reflectance (ATR-FTIR) and diffuse reflectance (DRIFT) spectroscopy to study selenate adsorption mechanisms on amorphous iron oxides and concluded that selenate adsorbs via a mixture of monodentate and bidentate inner-sphere complexes under aqueous conditions and forms bidentate inner-sphere complexes when dried. Wijnja and Schulthess (*15*) utilized both ATR-FTIR and Raman spectroscopy to investigate selenate and sulfate adsorption mechanisms on goethite in situ. They found that selenate and sulfate adsorb to goethite via the same mechanisms and that at pH 6.0 and above the adsorption occurs via an outer-sphere surface complexation mechanism. At pH below 6.0, inner-sphere monodentate surface complexes were observed. This is consistent with results of Peak et al. (*16*), who determined that between pH 6 and pH 9 sulfate forms only outer-sphere surface complexes on goethite, while at pH below 6.0 both outer- and inner-sphere surface complexes are formed on the goethite surface.

It was the hypothesis of our research that differences in selenate adsorption mechanisms observed in spectroscopic

* Corresponding author phone: (302)831-1595; fax: (302)831-0605; e-mail: dpeak@udel.edu.

10.1021/es0156643 CCC: $22.00
Published on Web 02/20/2002

studies from the literature could be explained by differences in reaction conditions in the studies. The objectives of this study were therefore to determine the effects that pH, surface loading, and ionic strength have on adsorption mechanisms of selenate on iron(III) oxides and hydroxides. Goethite, hematite, and amorphous iron hydroxide were the sorbents chosen due to their important differences in structure and their ubiquity in soils. EXAFS was the primary spectroscopic tool chosen due to its suitability to determine local bonding environments of selenate on all three sorbent phases. Additional information about selenate adsorption mechanisms on hematite was obtained using ATR-FTIR spectroscopy.

Materials and Methods

Mineral Synthesis. The goethite used in this study was synthesized using the method of Schwertmann et al. (*17*). Initially, ferrihydrite was precipitated by adding 50 mL of 1 M ferric nitrate solution to 450 mL of 1 M KOH. This suspension of amorphous hydrous ferric oxide was then aged for 14 days at 25 °C. The suspension was washed with doubly deionized water via centrifugation, resuspended in 0.4 M HCl, and shaken for 2 h using a mechanical shaker to remove any residual amorphous iron oxides from the surface of the goethite. The acidified goethite suspension was again washed with doubly deionized water to remove HCl and dissolved iron, dialyzed until the conductivity of the solution was equal to distilled water, frozen with liquid nitrogen, and freeze-dried. The solid was confirmed as goethite via infrared spectroscopy using both ATR and transmission mode KBr pellets. The external surface area determined from N_2-BET was 63.5 $m^2\ g^{-1}$. The hematite used in these experiments was synthesized from ferric perchlorate using the method of Schwertmann and Cornell (*18*). It was acid-washed, dialyzed, and freeze-dried following the same procedure described above for goethite and had an N_2-BET surface area of 14 $m^2\ g^{-1}$. Ferrihydrite (hydrous ferric oxide) was synthesized by titrating 1 M ferric chloride to pH 7.5 with 1 M KOH. This precipitate was washed 3 times with 0.1 M NaCl to remove any residual iron, washed once with deionized water, and then dialyzed for 3 days in deionized water. Rather than freeze-drying, the ferrihydrite was kept as a 10 g/L suspension and placed into a refrigerator to slow conversion to crystalline forms.

Sorption Experiments. All reactions of selenate with iron oxides were conducted in acid-washed 50-mL polypropylene centrifuge tubes. All chemicals used in sorption experiments were reagent grade or better. Reactants were added with electronic pipets (Rainen) that were calibrated with an analytical balance using the mass of deionized water at current laboratory temperature prior to sample preparation. Goethite and hematite were added to reaction tubes from a concentrated (50 g/L) suspension prepared from distilled deionized water, sonified to thoroughly mix, and then stirred while aliquots were being transferred. A solid density of 10 g/L was used for the hematite and goethite experiments, and a solid density of 2.5 g/L was used in the ferrihydrite samples. The ferrihydrite stock suspension was allowed to return to room temperature prior to sample preparation and then added from the well-stirred stock suspension. Water and a portion of the required background electrolyte were next added. Background electrolyte (NaCl) was added from a 1 M stock solution; 50 μL less NaCl than the amount desired for the final ionic strength was initially added. This allowed for HCl to be used for pH adjustment without affecting ionic strength of the final sample. Once the selenate was added to the reaction tubes and pH was adjusted to the desired value with 1 M HCl, the necessary background electrolyte (50 μL minus the amount of HCl used in μL) was finally added to the reaction vessels to adjust to the appropriate ionic strength. Samples were continuously mixed on a rotating shaker, and at 8 and 20 h, the sample pH was measured and adjusted to the desired value with 0.1 M HCl. After 24 h, the sample pH was recorded, and the samples were then centrifuged at 15 000 rpm for 10 min. The supernatant was filtered through a 0.2-μm filter and then analyzed for residual selenate via AAS (Perkin-Elmer model), while the solid was sealed in containers and refrigerated until EXAFS analysis.

EXAFS Spectroscopy. EXAFS spectra were collected at the Se K edge (12.658 keV) at Beamline X11-A of the National Synchrotron Light Source at Brookhaven National Laboratory. The electron storage ring was operating at either 2.5 or 2.8 GeV, depending on the date of spectral collection. The monochromator used in all experiments was a Si(111) crystal, and a slit width of 0.5 mm was used before the monochromator. This allowed for a spectral resolution of approximately 0.5 eV. Calibration was done to a 10 wt % elemental selenium standard, and detuning 30% at 900 eV past the Se edge minimized the effect of higher order harmonics. All samples were scanned in fluorescence mode using a Lytle detector with a Krypton-filled ionization chamber. The sample chamber was designed so that samples were placed at a 45° angle to the incident beam, and a wide-angle collector was 90° to the incident beam. An arsenic filter was placed between the sample compartment and the ionization chamber to eliminate elastically scattered X-rays from entering the ionization chamber. Additionally, several thicknesses of aluminum foil were placed in front of the arsenic filter to reduce Fe Kα radiation (*19*). To ensure adequate signal-to-noise for data analysis, three scans per sample were collected.

EXAFS Spectral Analysis. WinXAS versions 1.1 and 1.3 were used for all data analysis. Individual spectra were first averaged, and then backgrounds were subtracted by fitting a first order polynomial to the pre-edge region and a second order polynomial to the post-edge region. The resulting normalized spectra all have an edge jump of unity. Next, the normalized spectra were converted to a raw χ function. This was accomplished by setting E_0 equal to the inflection point of the second derivative of the normalized spectra to produce a μ function. Finally, a cubic spline was fitted to the μ function that was also weighted by k^3 to compensate for dampening of the EXAFS spectra at higher k ranges. This function was then Fourier transformed with a Bessel window and choosing end points at nodes of the function to produce the radial structure functions (RSF) that are presented in this paper. The k^3-weighted χ functions were also fitted to theoretical scattering paths using FEFF7 code. For the fitting, an amplitude reduction factor was fixed to 0.93; a value that was obtained by fixing the Se−O coordination number to 4.0 when fitting diluted sodium selenate salt. When fitting EXAFS samples, coordination numbers, bond lengths, and Debye−Waller factors were allowed to vary. E_0 shifts were constrained to be equal for both the Se−O and the Se−Fe scattering paths.

ATR-FTIR Spectroscopy. A Perkin-Elmer 1720x spectrometer was used for all infrared analysis. The spectrometer was equipped with a Whatman purge gas generator to remove CO_2(g) and H_2O(g) from the sample compartment, and a N_2(l)-cooled MCT detector was employed for data collection. A horizontal ATR sampling accessory and a trough-style sample holder with 45 ZnSe crystal (Spectra Tech) was utilized for sample analysis. For the aqueous SeO_4 standard, a 10 mM SeO_4/D_2O solution and a pure D_2O were analyzed, and then pure D_2O was subtracted from the standard to produce a spectrum of aqueous selenate. For the adsorption sample, hematite was deposited on the ZnSe crystal according to ref *24*, and then 1.5 mL of a background solution of 0.01 M NaCl in D_2O at a pD of 3.5 was placed in the trough over the deposit. The hematite was allowed to equilibrate with the solution for 1 h, a background spectrum was collected, and then 1.5 mL of a D_2O solution containing 500 mM SeO_4 and 0.01 M

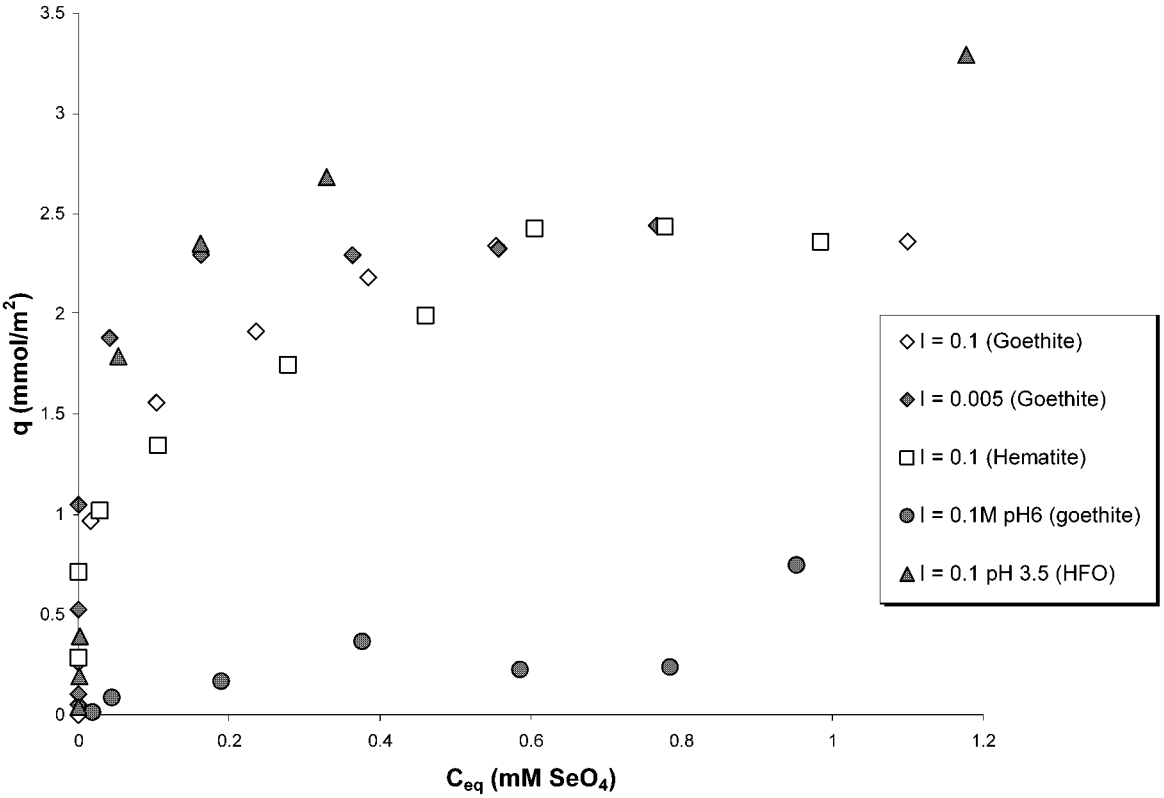

FIGURE 1. Adsorption isotherms for selenate sorbed on HFO, goethite, and hematite. All isotherms were conducted at pH 3.5 unless otherwise noted, and an ionic strength of either 0.005 or 0.1 M (NaCl) was used in all isotherms. These reaction conditions are identical to those chosen for EXAFS studies. It is possible to estimate q_{max} from the isotherms to be ~2.5 μmol/m^2 for SeO_4 on both hematite and goethite at pH 3.5; ~0.5 μmol/m^2 for SeO_4 on goethite at pH 6.0; and ~3.5 μmol/m^2 for SeO_4 on HFO at pH 3.5.

NaCl was added to the trough. This solution was allowed to mix and react for 2 h, and then a spectrum was collected of the adsorbed selenate. For all spectra, 1000 scans were collected at a resolution of 4 cm^{-1}. A linear baseline was fit to all samples with Galactic Peaksolve.

Results and Discussion

Macroscopic Studies. Figure 1 shows the results from adsorption isotherms of selenate on HFO, goethite, and hematite at several different reaction conditions. In all isotherms, Langmuir-type adsorption was observed. For goethite at pH 3.5 and an ionic strength of 0.1 and 0.005 M and for hematite at pH 3.5, a sorption maximum (q_{max}) at approximately 2.5 μmol/m^2 was observed in the isotherms. This suggests that the density of sites reactive with selenate must be very similar for these two crystalline iron oxides. At pH 6.0, the q_{max} for selenate on goethite was much lower, occurring at approximately 0.5 μmol/m^2. This is reasonable since the number of fully protonated surface sites on the goethite surface is much lower at pH 6 than it is at pH 3.5. In the case of HFO at pH 3.5, q_{max} was estimated at 3.5 μmol/m^2. For EXAFS spectroscopic studies, sample loadings will be expressed as a fraction of the sorption maximum or q/q_{max}.

EXAFS Spectroscopy. (a) Selenate Adsorption on Goethite. On the basis of results of in situ spectroscopic studies investigating sulfate (*15*, *16*) and selenate (*15*) adsorption on goethite, one would expect that pH, ionic strength, and surface loading all affect selenate adsorption mechanisms on goethite. Figure 2 shows the results of varying pH on selenate adsorption. In Figure 2a, the raw and fitted k^3-weighted χ data are shown, and in Figure 2b, the RSFs are seen. As expected, the spectra of aqueous selenate (spectrum a) can be completely described with a single shell fit using four oxygen atoms at a distance of 1.64 Å. Similarly, the spectrum of selenate adsorbed at pH 6.0 can also be adequately fit using parameters identical to aqueous selenate. Therefore at pH 6.0, selenate adsorbs on the goethite surface via formation of an outer-sphere surface complex. At pH 3.5 (spectra c and d), however, the spectrum can no longer be fully described with a single oxygen shell. This is clearly shown in spectrum c, as there are several features in the raw data that cannot be fit with an oxygen backscatterer. If one analyzes the same spectrum with a two-shell fit that includes an iron second shell with 1.5 Fe atoms at 3.31 Å (spectrum d), then the fit quality is improved and the spectrum can then be described. This demonstrates that, at pH 3.5, inner-sphere complexation of selenate occurs on the goethite surface.

The effect that pH has on changing selenate adsorption mechanisms on goethite is quite dramatic, but other reaction conditions such as ionic strength and surface loading have a more subtle effect. Figure 3a shows the effect of changing ionic strength from 0.005 to 1.0 M while maintaining a surface loading of 1.56 μmol/m^2 and a pH of 3.5. The spectra at both 1 and 0.1 M ionic strength appear virtually identical, with 1.5 Fe atoms at a distance of 3.31 Å indicating inner-sphere complexation. At 0.005 M ionic strength, however, the second shell was too weak to fit consistently, although some contribution of Fe can be seen in the RSF. Figure 3b demonstrates that, as surface loading is changed by a factor of 5 (from 0.78 to 2.5 μmol/m^2) while ionic strength and pH are kept constant (0.1 M and pH 3.5, respectively), no change in bond distances of selenate can be observed with EXAFS. This suggests that the same complexation mechanism is occurring as loading changes.

Perhaps a large part of the discrepancies between the work of Hayes and co-workers (*13*) and that of Manceau and Charlet (*14*) can be described by differences in the ionic strength in the samples that they studied. Manceau and

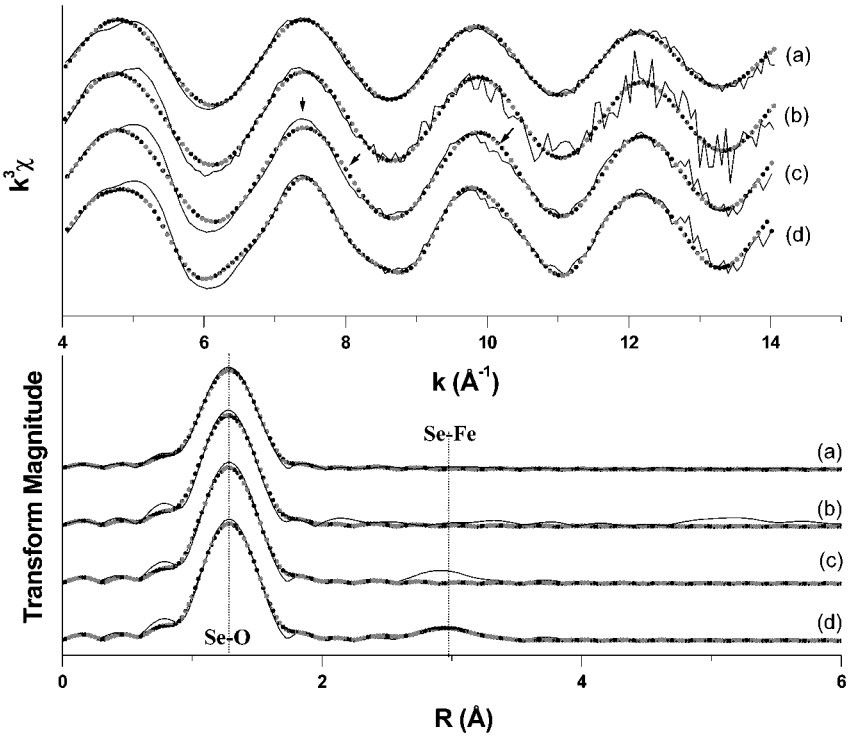

FIGURE 2. EXAFS spectra of selenate adsorbed on goethite at loading of 1.56 μmol/m^2 and ionic strength of 0.1 M. Solid lines representing the raw data, and the dotted lines are the fits to the data. The upper figure shows the raw k^3 weighted χ data, and the lower figure shows RSFs. The spectra are as follows: (a) 10 mM SeO_4 and a single shell fit of 4 oxygens at 1.64 Å, (b) 1 mM SeO_4 adsorbed at pH 6.0 and a single shell fit of 4 oxygens at 1.64 Å, (c) 1 mM SeO_4 adsorbed at pH 3.5 and a single shell fit of 4 oxygens at 1.64 Å, (d) 1 mM SeO_4 adsorbed at pH 3.5 and a two shell fit of 4 oxygens at 1.64 Å and 1.5 Fe at 3.31 Å. Note the features in the raw χ data of spectrum 1c pointed out with arrows where a single shell fit is unable to describe the pH 3.5 spectrum. When a second shell arising from Fe backscattering is added to the fitting procedure (1d), these features in the χ data are reproduced.

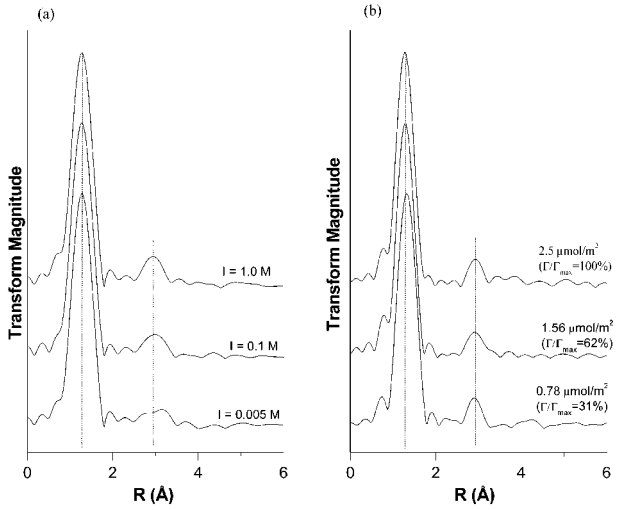

FIGURE 3. RSFs of selenate adsorbed on goethite at pH 3.5 as a function of (a) ionic strength and (b) surface loading. In panel a, all samples have a surface loading of 1.56 μmol/m^2 Se (~60% Γ/Γ_{max}). It can clearly be seen that as ionic strength is lowered from 1.0 to 0.005 M and that the contribution of iron to the RSF becomes less important. This is evidence of increased outer-sphere complexation at low ionic strength. In panel b, ionic strength was held at 0.1 M and surface coverage of selenate was varied. Loading (Γ/Γ_{max}) varied from 31 to 100% of the maximum loading from an adsorption isotherm conducted under the same conditions.

Charlet (*14*) conducted all experiments at an ionic strength of 0.1 M $NaNO_3$ and a pH of 3.5, and Hayes and co-workers also studied adsorption at a pH of 3.5 but did not report ionic strength (*13*). Another possibility is that EXAFS analysis of selenate adsorption on iron oxides requires good data quality out to high k range as mentioned in ref *14*. EXAFS spectra of selenite adsorbed on iron oxides produces χ spectra that are completely out of phase from aqueous selenite, while adsorbed selenate χ spectra have dampening and destructive interferences that are much subtler.

(b) Selenate Adsorption on Other Iron Oxides. Figure 4 shows Fourier transformed spectra of several selenate reference spectra as well as selenate sorbed on goethite, hematite, and HFO at pH 3.5, an ionic strength of 0.1 M, and a surface loading of 3700 mg of Se/kg of sorbent. For aqueous selenate, one can readily see that the only structure is a single shell of four oxygen atoms at 1.64 Å. This is expected for the tetrahedral selenate molecule, and the observed Se−O bond distance is in good agreement with other EXAFS studies (*13*, *14*, *20*). For selenate-substituted schwertmannite, the central Se still has a tetrahedral coordination with a Se−O bond distance of 1.64 Å, but an additional contribution from Fe is also observed at 3.32 Å. This can be interpreted in several ways. Schwertmannite is an iron(III) oxyhydroxy sulfate, with a tunnel structure that is similar to akageneite (*21*). The actual bonding environment of sulfate in the tunnels is still the subject of debate. It is possible that the observed second shell is due to structural selenate, but the observed bond distance of 3.34 Å would place a large strain on the mineral's structure. An alternative explanation is that there are two bonding environments for selenate in the substituted schwertmannite: structural and sorbed. The structural selenate can then be present as the more favorable (from a crystallographic standpoint) outer-sphere counterion in the tunnels, while the sorbed selenate can form inner-sphere complexes on the surface that are seen with EXAFS spectroscopy. This is consistent with the in situ ATR-FTIR spectroscopic studies of sulfate bonding in schwertmannite

TABLE 1. Structural Parameters of SeO_4 Sorbed on Iron Oxides and Parameters for Reference Selenate Compounds

				first shell			second shell		
				Se−O			Se−Fe		
sorbent	loading (μmol/m^2)	q/q_{max} (%)	reaction conditions	R (Å)[a,d]	N[b,f]	$\Delta\sigma^2$ (Å^2)[c,e]	R (Å)[d]	N[e]	$\Delta\sigma^2$ (Å^2)[e]
goethite	1.56	62%	pH 3.5, $I = 1$	1.64	4	0.02	3.31	1.2	0.005
goethite	1.56	62%	pH 3.5, $I = 0.1$	1.64	4	0.0020	3.32	1.6	0.008
goethite	1.56	62%	pH 3.5, $I = 0.005$	1.64	4	0.0008			
goethite	0.50	100%	pH 6.0, $I = 0.1$	1.64	4	0.0040			
goethite	0.78	31%	pH 3.5, $I = 0.1$	1.64	4	0.0020	3.31	1.5	0.008
goethite	2.50	100%	pH 3.5, $I = 0.1$	1.64	4	0.0030	3.31	1.3	0.007
hematite	0.78	31%	pH 3.5, $I = 0.1$	1.65	4	0.004	3.3	1.7	0.001
HFO	0.78	31%	pH 3.5, $I = 0.1$	1.64	4	0.0020	3.30	1.87	0.0090
references									
Se−schwertmannite				1.64	4	0.0060			
aqueous SeO_4^{2-}				1.64	4	0.0070			
Na_2SeO_4 salt				1.64	4	0.002			

[a] Interatomic distance. [b] Coordination number. [c] Debye-Waller factor fit quality estimated accuracy. [d] ±0.02 Å. [e] ±20%.

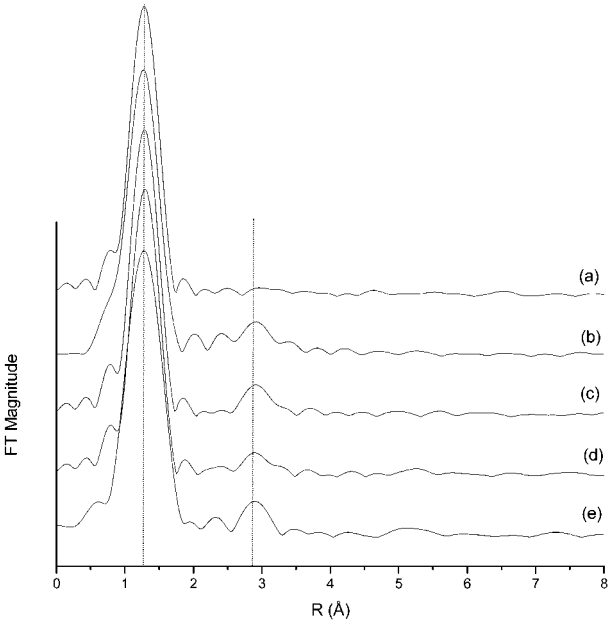

FIGURE 4. RSFs for 10 mM SeO_4^{2-}(aq) (a), SeO_4-substituted schwertmannite (b), and SeO_4 adsorbed on (c) goethite, (d) HFO, and (e) hematite. For all three adsorption samples, pH 3.5, $I = 0.1$ M, and 1.56 μmol/m^2 SeO_4 were used.

(*16*), which showed both outer-sphere sulfate and inner-sphere sulfate present. The spectrum of Se-substituted schwertmannite in Figure 4 is quite consistent with the work of Waychunas et al. (*20*), who reported a mean Se−Fe distance of 3.37 Å. They found an improved fit with two Se−Fe distances, one longer and attributed to structural (tunnel) selenate and a second shorter bond distance for inner-sphere sorbed selenate. However, they did not report the fitted distances.

The adsorption samples on hematite, goethite, and HFO all contain inner-sphere selenate surface complexes. This can be clearly seen from the second shell that is observed in all the RSFs. The fit results from selenate adsorbed on different sorbents and on goethite under different reaction conditions are all compiled in Table 1. This second shell can be fitted with 1−1.5 Fe atoms at 3.31−3.33 Å depending on the sorbent. In the goethite and HFO samples, another weak shell can be seen in the RSF at a slightly longer bond distance but was not significant enough to fit with precision. The position is similar to the distance observed in Se-substituted schwertmannite as well. The presence of inner-sphere selenate on goethite is consistent with the work of Manceau and Charlet (*14*), and they reported a similar Se−Fe bond distance of 3.29 Å as compared to 3.31 Å in this work. On hydrous ferric oxide (HFO), however, they found that their data were best described with 0.4 Fe at 2.80 Å and 1.8 Fe at 3.29 Å. They attributed the distance of 2.80 Å to an edge-sharing (bidentate mononuclear) surface complex and the distance of 3.29 Å to that of a corner-sharing (bidentate binuclear) surface complex. This feature was not observed in our EXAFS samples, but there were differences in the reaction conditions between our study and Manceau and Charlet (*14*). First of all, the sorption experiments of Manceau and Charlet were conducted on fresh (non-freeze-dried) HFO that all had Se loadings of 1.3 wt % Se, whereas the selenate sorption samples on HFO in this study contained only 0.37 wt % Se. The tendency of selenate to form edge-sharing complexes on HFO may be dependent upon the surface loading, with less favorable surface sites becoming more active in adsorption as surface loading increases. A second difference is the background electrolyte, NaCl in this study versus $NaNO_3$ in Manceau and Charlet (*14*). Chloride is not an indifferent electrolyte (*22*) and could possibly affect the tendency of SeO_4 to react with the edge sharing sites of HFO. We used a background of sodium chloride to be able to compare our results with ATR-FTIR spectroscopic studies and also with previous ATR-FTIR (*12*, *15*, *16*) and Raman (*16*) spectroscopic analysis of sulfate adsorption on iron oxides and hydroxides. Finally, our HFO sample was prepared from ferric chloride (to avoid nitrate contamination), and it is possible that the presence of chloride affects the structure of the amorphous HFO gel.

Selenate ATR-FTIR Spectroscopic Studies. Vibrational spectroscopy is a useful complementary technique to EXAFS spectroscopy because several structural configurations of oxyanions (for example, monodentate vs bidentate) may result in similar Se−Fe bond lengths depending on the bond angles and geometry and the amount of distortion of the oxyanion tetrahedron. However, the different possible surface complexes will result in different molecular symmetries and therefore quite different vibrational spectra. Figure 5 shows the spectrum of aqueous selenate (in D_2O) as compared to a spectrum of selenate adsorbed to hematite at pD 3.5, an ionic strength of 0.1 M, and an initial SeO_4 concentration of 250 μM. For aqueous SeO_4, there is only one broad peak occurring at 865 cm^{-1}. This peak corresponds to the infrared-active symmetric stretching ν_3 band of tetrahedral (T_d) SeO_4 molecule. When adsorbed on hematite at pD 3.5, selenate has a symmetry of C_{3v}, with the ν_3 splitting to two peaks at

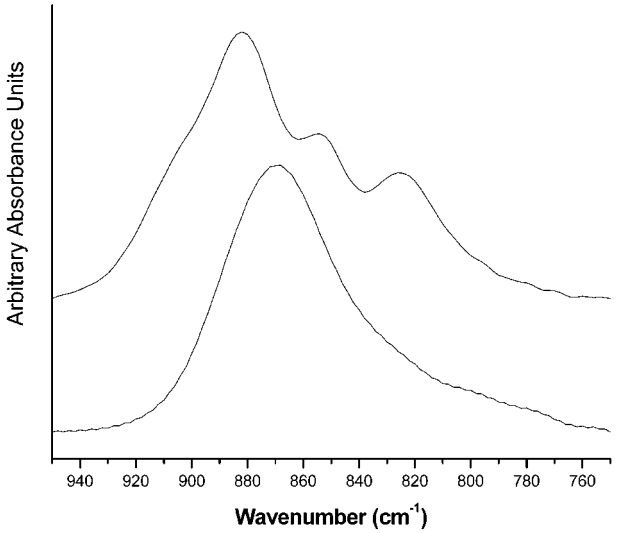

FIGURE 5. ATR−FTIR spectra of (a) selenate adsorbed on hematite at pD 3.5, $I = 0.1$ M, and $C_{eq} = 250\ \mu$M SeO_4 and (b) 10 mM SeO_4^{2-}(aq). Spectra are the result of 1000 co-added scans at 4 cm^{-1} resolution.

880 and 850 cm^{-1} and the ν_1 peak at 820 cm^{-1} becoming infrared active. The observed C_{3v} symmetry is the result of a monodentate selenate surface complex, which has previously been observed for sulfate adsorption on hematite (*12*). Unfortunately, ATR-FTIR experiments using goethite and HFO as the sorbent phase were unsuccessful due to overlap of infrared peaks of the iron oxides with the Se−O vibrational modes. Even without direct ATR-FTIR spectroscopic studies, it is reasonable to conclude that, since selenate and sulfate both form monodentate complexes on hematite, selenate can be expected to form the same types of surface complexes on goethite and HFO as does sulfate. A sulfate monodentate inner-sphere surface complex has previously been observed at low pH on goethite by several researchers (*15*, *16*, *23*). An additional component of hydrogen bonding to an adjacent surface site is sometimes proposed rather than a simple monodentate surface complex (*16*, *23*). Hydrogen bonding can easily be seen with vibrational spectroscopy due to the effects that the proton has on the vibration of the adjacent Se−O bond, but it is unlikely to affect the EXAFS spectra enough to be observable since a proton is not likely to change bond distances between Se and Fe. Hydrogen bonding to an adjacent site would also tend to bring the selenate tetrahedron closer to the surface and therefore produce Se−Fe bond distances intermediate between monodentate and bidentate. This lends credence to our assignment of a monodentate inner-sphere surface complex for SeO_4 adsorbed to iron oxides at pH 3.5. Wijnja and Schulthess (*16*) used Raman spectroscopy to study SeO_4 adsorption on goethite and found outer-sphere complexation at pH 6.0 and above and an inner-sphere monodentate surface complex at pH below 6.0. This is in good agreement with our EXAFS results in this study as well as consistent with previous in situ spectroscopic studies of sulfate adsorption on goethite.

Importance of Outer-Sphere Adsorption. One of the primary goals of this research was to investigate the continuum between outer-sphere and inner-sphere complexation of selenate on different iron oxides. This continuum of adsorption mechanisms is difficult to demonstrate with EXAFS spectroscopy, as the only effect that increasing the ratio of outer-sphere to inner-sphere surface complexes has on Se EXAFS spectra is a decrease in the intensity of iron contribution in the Fourier transforms. As outer-sphere selenate concentrations increase, the Se−Fe contribution to the overall spectra is being diluted by adding only more Se−O signal since no iron backscattering can be seen from the outer-sphere selenate. All comparisons of second shell intensities should made with caution, as there is a large error in the intensity associated with RSFs. However, there is no other way to judge the contribution of outer-sphere selenate to the overall adsorption mechanism. If one looks at the RSFs in Figures 2 and 3, then it becomes clear that as pH increases from 3.5 to 6.0, the importance of inner-sphere selenate to the EXAFS spectrum decreases. Similarly, as ionic strength is decreased from 1 to 0.005 M, one can see that there is less inner-sphere selenate on goethite. This is consistent with the continuum of adsorption mechanisms proposed for sulfate adsorption on goethite (*13*). Figure 4 also displays a similar trend when compared to sulfate FTIR data. In the case of hematite, only inner-sphere monodentate surface complexes are seen, and the EXAFS spectrum of selenate on hematite has a single strong well-defined second shell. In the case of HFO, the second shell is much less prominent; suggesting that while there is inner-sphere selenate, there is also a substantial outer-sphere component. This is consistent with ATR-FTIR spectroscopic studies of sulfate adsorption on HFO (*21*), where it was observed that complexation mechanisms are similar between goethite and HFO but that HFO had a much larger amount of outer-sphere sulfate complexation. So while the exact amount of outer-sphere selenate is impossible to determine with EXAFS, the relative size and order of the second shell observed in all our spectra seem consistent with a mixture of outer- and inner-sphere selenate on goethite and HFO that is affected by pH and ionic strength. No noticeable change occurs with surface loading (Figure 3b) at low pH, suggesting that, at least for selenate, this reaction variable is less important in determining adsorption mechanisms than pH or ionic strength.

It is becoming increasingly clear that adsorption mechanisms of oxyanions on metal oxides need not be either outer-sphere or inner-sphere but instead can be a mixture of both. It was theorized by Sposito (*24*) that some oxyanions such as sulfate adsorb with intermediate strength, sometimes forming inner-sphere complexes and sometimes forming outer-sphere complexes. This continuum of adsorption mechanisms has been demonstrated with direct spectroscopic evidence in the case of sulfate adsorption on goethite (*15*, *16*, *25*, *26*) and HFO (*24*), selenate adsorption on goethite (*14*), and arsenite adsorption on aluminum oxides (*27*) and iron oxides (*28*). It is therefore of vital importance to widely vary reaction variables such as pH, ionic strength, and surface loading in sorption experiments to accurately describe the effects that reaction conditions have on the distribution of adsorption mechanisms. Environmental scientists who are developing surface complexation and larger-scale transport models can then use this complete understanding of how oxyanions adsorb over all reaction conditions.

Acknowledgments

D.P. thanks the National Science Foundation for support via a graduate fellowship, Dr. Andreas Scheinost for providing early guidance in EXAFS data analysis, and the staff at NSLS beamline X11-A for assistance in data collection and experimental setup.

Literature Cited

(1) Zhang, P. C.; Sparks D. L. *Environ. Sci. Technol.* **1990**, *24*, 1848−1856.
(2) Shriver, D. F., Atkins P. A., Langford C. H. *Inorganic Chemistry*; W. H. Freeman and Company: New York, 1994.
(3) Stumm, W.; Morgan, J. J. *Aquatic Chemistry*; John Wiley and Sons: New York, 1996.
(4) Ahlrichs, J. S.; Hossner, L. R. *J. Environ. Qual.* **1987**, *16* (2), 95−98.
(5) Bar-Yosef, B.; Meek, D. *Soil Sci.* **1987**, *144* (1), 11−19.
(6) Neal, R. H.; Sposito, G. S. *Soil Sci. Soc. Am. J.* **1989**, *53*, 70−74.

(7) Davis, J. A.; Leckie J. O. *J. Colloid Interface Sci.* **1980**, *74*, 32−43.
(8) Yamaguchi, N. U.; Okazaki, M.; Hashitani, T. *J. Colloid Interface Sci.* **1999**, *209*, 386−391.
(9) Su, C.; Suarez, D. L. *Soil Sci. Soc. Am. J.* **2000**, *64*, 101−111.
(10) Harrison, J. B.; Berkheiser, V. E. *Clays Clay Miner.* **1982**, *30*, 97−102.
(11) Johnston, C. T.; Sposito, G. In *Future Developments in Soil Science Research*; Boersma, L. L., Ed.; Soil Science Society of America: Madison, WI, 1987.
(12) Hug, S. J. *J. Colloid Interface Sci.* **1997**, *188*, 415−422.
(13) Hayes, K. F.; Roe A. L.; Brown G. E.; Hodgen K. O.; Leckie J. O.; Parks G. A. *Science* **1987**, *238*, 783−786.
(14) Manceau, A.; Charlet L. *J. Colloid Interface Sci.* **1994**, *168*, 87−93.
(15) Wijnja, H.; Schulthess C. P. *J. Colloid Interface Sci.* **2000**, *229*, 286−297.
(16) Peak, D.; Ford, R. G.; Sparks, D. L. *J. Colloid Interface Sci.* **1999**, *218*, 289−299.
(17) Schwertmann, U.; Cambier P.; Murad E. *Clays Clay Miner.* **1985**, *33* (5), 369−378.
(18) Schwertmann, U.; Cornell, R. M. *Iron Oxides in the Laboratory: Preparation and Characterization*; VCH: Weinheim, New York, 1991
(19) Bargar, J. R.; Brown, G. E., Jr.; Parks, G. A. *Geochim. Cosmochim. Acta* **1997**, *61*, 2639−2652.
(20) Waychunas, G. A.; Xu, N.; Fuller, C. C.; Davis, J. A.; Bigham, J. M. *Physica B* **1995**, *208/209*, 481−483.
(21) Bigham, J. M.; Schwertmann, U.; Carlson, L.; Murad, E. *Geochim. Cosmochim. Acta* **1990**, *54*, 2743.
(22) Bargar J. R.; Brown, G. E., Jr.; Parks, G. A. *Geochim. Cosmochim. Acta* **1998**, *62*, 193−207.
(23) Ostergren, J. D.; Brown, G. E., Jr.; Parks, G. A.; Persson, P. *J. Colloid Interface Sci.* **2000**, *225*, 483−493.
(24) Sposito, G. *The Surface Chemistry of Soils*; Oxford University Press: New York, 1984.
(25) Peak, D.; Elzinga, E. J.; Sparks, D. L. *Heavy Metals Release in Soils*; Selim, H. M., Sparks, D. L., Eds.; Lewis Publishers: Boca Raton, FL, 2001.
(26) Elzinga, E. J.; Peak, D.; Sparks, D. L. *Geochim. Cosmochim. Acta* **2001**, *65*, 2219−2230.
(27) Arai, Y. A.; Elzinga, E. J.; Sparks, D. L. *J. Colloid Interface Sci.* **2001**, *235*, 80−88.
(28) Goldberg, S.; Johnston, C. T. *J. Colloid Interface Sci.* **2001**, *234*, 204−216.

Received for review August 24, 2001. Revised manuscript received January 2, 2002. Accepted January 4, 2002.

ES0156643